β-decay half-lives and β-delayed neutron multiplicities of the neutron drip-line nuclei ^{19}B, ^{22}C, and ^{23}N

K. Yoneda,[1,*] N. Aoi,[1] H. Iwasaki,[1] H. Sakurai,[2] H. Ogawa,[3] T. Nakamura,[1] W.-D. Schmidt-Ott,[4] M. Schäfer,[4] M. Notani,[2] N. Fukuda,[1] E. Ideguchi,[2] T. Kishida,[2] S. S. Yamamoto,[5] and M. Ishihara[1,2]

[1]*Department of Physics, University of Tokyo, 7-3-1 Hongo, Bunkyo-ku, Tokyo 113-0033, Japan*

[2]*RIKEN (The Institute of Physical and Chemical Research), Hirosawa 2-1, Wako-shi, Saitama 351-0198, Japan*

[3]*Department of Physics, Tokyo Institute of Technology, Oh-Okayama 2-12-1, Meguro-ku, Tokyo 152-8551, Japan*

[4]*Zweites Physikalisches Institut der Universität Göttingen, Bunsenstrasse. 7-9, D-37037 Göttingen, Germany*

[5]*Department of Physics, Sophia University, 7-1 Kioi-cho, Chiyoda-ku, Tokyo 102-0094, Japan*

(Received 9 August 2002; published 27 January 2003)

Beta-decay properties of the neutron drip-line nuclei ^{19}B, ^{22}C, and ^{23}N have been studied using projectile fragments from 95 MeV/nucleon ^{40}Ar ions incident on a ^{nat}Ta target. The β-decay half-lives of ^{22}C and ^{23}N have been determined for the first time to be $6.1^{+1.4}_{-1.2}$ and $14.1^{+1.2}_{-1.5}$ ms, respectively. The half-life of ^{19}B was reinvestigated, resulting in a new value of 2.92 ± 0.13 ms. The β-delayed neutron multiplicities have also been determined to be $P_{1n}=71.8^{+8.3}_{-9.1}$%, $P_{2n}=16.0^{+5.6}_{-4.8}$% for ^{19}B, $P_{1n}=61^{+14}_{-13}$% for ^{22}C, and $P_{1n}=42.2^{+6.3}_{-6.5}$%, $P_{2n}=8.0^{+3.8}_{-3.4}$% for ^{23}N. The results are compared with theoretical predictions.

DOI: 10.1103/PhysRevC.67.014316 PACS number(s): 21.10.Tg, 23.40.−s, 27.20.+n, 27.30.+t

I. INTRODUCTION

In recent years a vast number of isotopes near the neutron drip line have become accessible, and intensive experimental efforts have been devoted to explore the properties of neutron-rich nuclei. These nuclei often exhibit exotic phenomena, and shed interesting light on the basic mechanisms responsible for the nuclear stability and structure.

The fundamental procedure for such investigations is first to establish the existence of a new isotope. At present the boundary of the neutron stable nuclei has been established up to oxygen [1], while the heaviest isotopes so far identified are ^{31}F [1], ^{34}Ne [2], ^{37}Na [2], ^{38}Mg [3], ^{41}Al [3], and ^{43}Si [2] for the $Z=9-14$ elements. The present work is an attempt to broaden our knowledge of the basic characteristics of such drip-line isotopes. For this purpose the β-decay half-lives ($t_{1/2}$) and β-delayed neutron multiplicities (P_{in}: $i=0,1,2,\ldots$) were studied for ^{19}B, ^{22}C, and ^{23}N. These quantities depend, in particular, on the Q_β value of a parent nucleus and the neutron separation energies (S_{in}: $i=0,1,2,\ldots$) of the daughter nuclei. They are also related to the β-decay strength function of the Gamow-Teller transitions.

Experimental studies on very neutron-rich isotopes are often hampered by the small production rates. Among other observables, $t_{1/2}$ and P_{in} represent properties which can be determined with a very small production rate such as 10^{-3} s^{-1}. Nevertheless, the heaviest boron, carbon, and nitrogen isotopes with known $t_{1/2}$ values are ^{19}B, ^{20}C, and ^{22}N [4–6], while P_{in} data were only available up to ^{17}B, ^{20}C, and ^{22}N. In the present work, we have extended the measurement to the three drip-line nuclei, ^{19}B, ^{22}C, and ^{23}N, by employing a high-energy high-intensity ^{40}Ar beam and the large acceptance RIKEN projectile-fragment separator (RIPS) [7]. The use of ^{nat}Ta for the production target has also helped to enhance the production rates [8]. With all these merits combined, the useful yields of 5.5×10^{-2}, 5.3×10^{-3}, and 1.2×10^{-1} s^{-1} were obtained for ^{19}B, ^{22}C, and ^{23}N, respectively.

The isotopes studied are very neutron-rich nuclei so that they readily emit neutrons after the leading β decay. Even the emission of two neutrons may have a significant probability. Thus the β-ray spectra to be measured will be subject to a mixture of the successive β decays of the daughter nuclei. The separation of these different contributions has been facilitated by the relatively strong yields achieved, which have allowed us to obtain β-decay curves using not only the β rays detected in singles but also in coincidence with delayed neutrons. The values of $t_{1/2}$ and P_{in} were then deduced by fitting these curves consistently. In this analysis a careful fitting, including the background and daughter decay components, was essential. For this purpose we introduced a novel statistical treatment, in which the singles and coincidence decay curves were fitted simultaneously with a common set of parameters. The values of $t_{1/2}$ and P_{in} were among those parameters, and thus were determined automatically. This method was effective to reduce ambiguities in the deduced values of $t_{1/2}$ an P_{in}.

In this paper we present the results on the measurement of $t_{1/2}$ and P_{in} for ^{19}B, ^{22}C, and ^{23}N, which have been determined with good accuracy. These are reevaluated values of our preliminary results reported earlier [9]. In the course of the present experiment, the β decays of other neutron-rich isotopes, namely, ^{20}C and ^{22}N, were also studied. For the sake of calibration, we also performed a separate run to measure the β decay of ^{15}B, which has known values of $t_{1/2}$ [10] and P_{1n} [11].

*Present address: RIKEN (The Institute of Physical and Chemical Research), Hirosawa 2-1, Wako-shi, Saitama 351-0198, Japan. Electronic address: yoneda@rarfaxp.riken.go.jp

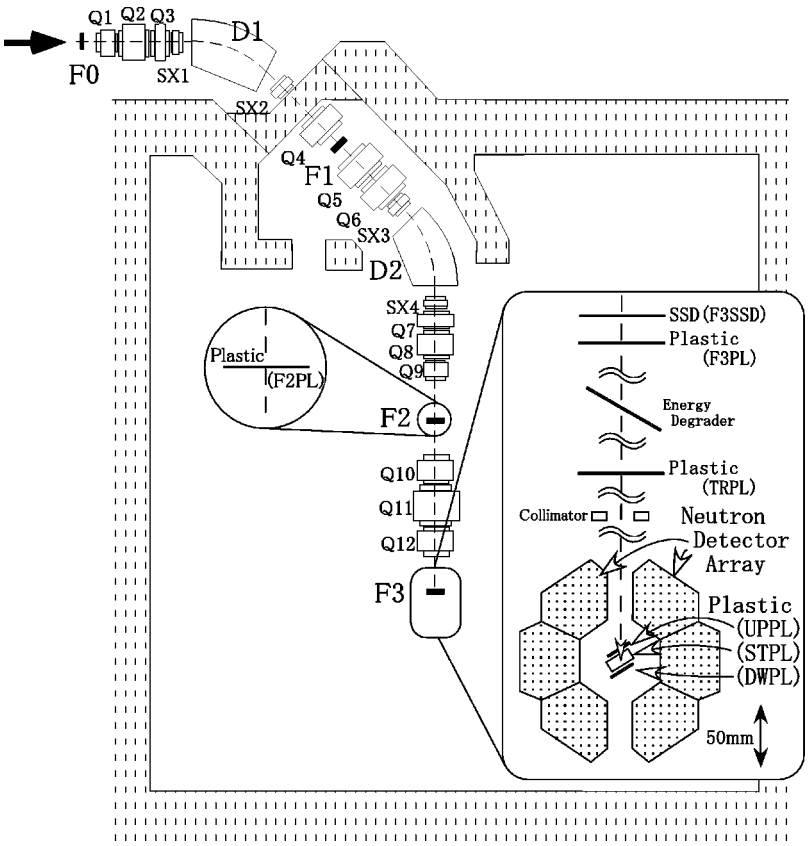

FIG. 1. A schematic view of the beam line and detector arrangement. The detectors for beam diagnosis were placed at the standard foci of RIPS, $F2$ and $F3$. The detectors for β-decay measurement were located around the final focus $F3$.

II. EXPERIMENT

The experiment was performed using RIPS at RIKEN Accelerator Research Facility. Neutron-rich boron, carbon, and nitrogen isotopes were produced by the fragmentation reaction of ^{40}Ar projectiles, and were implanted in an active stopper made of a plastic scintillation detector. Each of the incoming nuclei was identified in flight by time-of-flight (TOF) and energy-loss (ΔE) information. When a nucleus with $Z \geqslant 5$ was implanted, the primary beam was turned off for 100 ms. During the beam-off period, the β decay of the implanted nuclei was observed. Beta rays were detected by the active stopper, and β-delayed neutrons were detected in coincidence by a neutron detector array, which consisted of 13 liquid scintillation detectors. Decay curves were thus obtained for β-ray singles and β-neutron(s) coincidence events jointly to deduce $t_{1/2}$ and P_{in}. A schematic view of the experimental setup is shown in Fig. 1. In the following, the details of the detector setup and experimental techniques are described.

A. Isotope production

The neutron-rich boron, carbon, and nitrogen isotopes were produced by the projectile fragmentation reaction of a 95 MeV/nucleon ^{40}Ar beam on a 670 mg/cm^2 ^{nat}Ta target. The target thickness was chosen to maximize the yield of ^{22}C based on a semiempirical yield estimation by the INTENSITY code [12]. The reaction fragments were analyzed and collected through RIPS operated in an achromatic mode at the maximum solid angle (5 msr). We used three sets of magnetic rigidities, each optimized for ^{19}B, ^{22}C, and ^{23}N. An aluminum wedge degrader with a mean thickness of 583 mg/cm^2 was located at the momentum dispersive focus ($F1$) for the isotope separation.

The particle identification was performed event-by-event based on the TOF-ΔE information. The TOF was measured with two 1-mm-thick plastic scintillation detectors, $F2$PL and $F3$PL, which were located at the focal points $F2$ and $F3$, respectively. These detectors were about 6.5 m apart from each other. ΔE was measured by a 0.5-mm-thick silicon detector, $F3$SSD, placed at $F3$. A 2-mm-thick plastic scintillation detector, TRPL, was placed after $F3$PL. The energy deposit of the incoming particle in TRPL provided a measure of the Z of the fragment. TRPL afforded a quick response compared to $F3$SSD so that the former was used to provide a trigger signal as described in Sec. II D. On the other hand, a better resolution of $F3$SSD was employed to obtain a more definite identification of nuclei in the off-line analysis. In order to achieve sufficient power of isotope separation, the momentum acceptance of RIPS was limited by a slit at $F1$: full acceptance (6%) for ^{19}B and ^{22}C, and 4% acceptance for ^{23}N. Figure 2 shows a TOF versus ΔE plot obtained for the optimal RIPS setting for ^{19}B, which exhibits sufficient resolutions of TOF and ΔE for the separation of the neutron-rich isotopes in the $Z=5-7$ region.

B. Implantation of the nuclei

The fragments of interest were implanted in an active stopper (STPL) located at the final focus of RIPS ($F3$). The

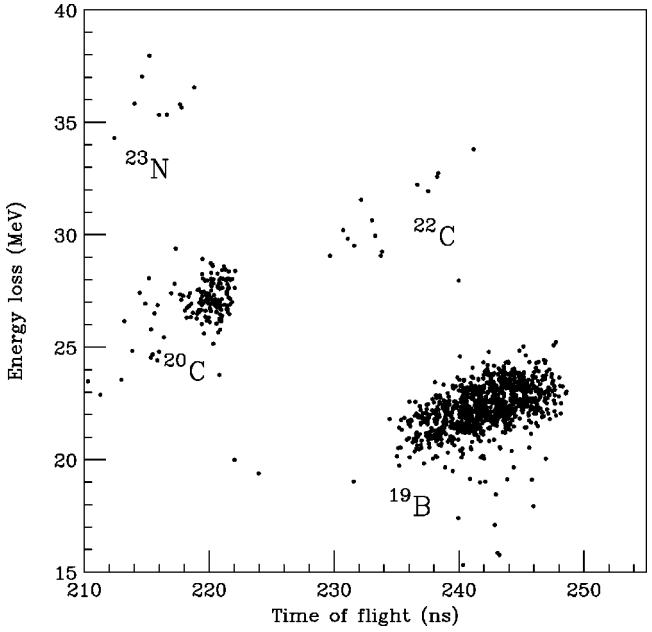

FIG. 2. A scatter plot of energy loss vs time-of-flight obtained in the optimal condition of RIPS for ^{19}B. Different isotopes are well separated from each other.

TABLE I. Numbers of nuclei implanted in the stopper plastic scintillation detector for each RIPS setting.

RIPS setting	Nucleus	Number of implanted nuclei (counts)
(a) Setting optimal for ^{19}B		
$B\rho_1 = 4.930\ T \cdot m$	^{19}B	1200
$B\rho_2 = 4.747\ T \cdot m$	^{20}C	170
Momentum acceptance: 6%	^{22}C	15
	^{23}N	9
(b) Setting optimal for ^{22}C		
$B\rho_1 = 4.754\ T \cdot m$	^{19}B	166
$B\rho_2 = 4.527\ T \cdot m$	^{20}C	17
Momentum acceptance: 6%	^{22}C	107
	^{23}N	19
(c) Setting optimal for ^{23}N		
$B\rho_1 = 4.238\ T \cdot m$	^{19}B	195
$B\rho_2 = 3.970\ T \cdot m$	^{20}C	85
Momentum acceptance: 4%	^{22}N	263
	^{23}N	2363

stopper was made of a 12-mm-thick plastic scintillation detector with an area of 40×35 mm^2. It was sandwiched by the upstream and downstream plastic scintillation detectors, UPPL and DWPL, which had a thickness of 2 mm each. These three detectors were aligned at a tilted angle to minimize interference with a neutron detector array described in Sec. II C.

An aluminum plate, operated as a rotatable energy degrader, was placed upstream of TRPL to control the range of incoming fragments in the stopper. The thickness and rotation angle of the aluminum plate were chosen so that the fragments of interest were stopped within the volume of STPL. This procedure was performed by monitoring signals from UPPL, STPL, and DWPL. The fragments of interest were implanted with high collection efficiencies and with good purities as listed in Table I. Fairly high implantation rates of 3.8×10^{-2}, 3.2×10^{-3}, and 8.7×10^{-2} s^{-1} were obtained for ^{19}B, ^{22}C, and ^{23}N, respectively, by employing the optimal setting for each nucleus.

C. Detector setup for β rays and neutrons

The β decay of an implanted isotope was observed by detecting β rays and delayed neutrons. Beta rays were detected by the active stopper STPL with a phototube attached to each end. The output of STPL provided a timing signal to register the time spectrum of β-decay events. By setting the threshold level of STPL at about 100 keV, most of the β rays (about 90%) from the implanted fragments were recorded.

Beta-delayed neutrons were detected in coincidence with β-rays using a neutron detector array placed around STPL. It consisted of 13 liquid scintillation detectors (Bicron BC501A), which covered a solid angle of about 80% of 4π. The distance from the center of STPL to the surface of the neutron detector array was 5 cm, and the length of the liquid scintillation detectors was about 7 cm. The energy threshold was set at 50 keV in equivalent electron energy E_{eq}. This corresponds to about 400 keV in neutron energy, and is compatible with values used for the earlier measurements of P_n [13]. A more detailed description of the neutron detector array can be found in Ref. [14].

These scintillation detectors were sensitive to γ rays as well as neutrons. To separate out neutrons we adopted two methods, depending on the amount of the total light output of each event. For a large light output with $E_{\mathrm{eq}} > 200$ keV, a pulse shape analysis was applied. Figure 3(a) shows a typical plot of the total light output versus the amount of light output integrated over the first 60 ns, obtained for the β decay of ^{15}B. Neutrons and γ rays are well separated by the different fractions of the fast and slow components of their light outputs. The area within the solid lines in Fig. 3(a) indicates the gate adopted for β-delayed neutron events. For a small light output with 50 keV $\leqslant E_{\mathrm{eq}} \leqslant 200$ keV, the TOF information was used to separate neutrons and γ rays. Figure 3(b) shows a TOF spectrum obtained in the ^{15}B β-decay measurement. The horizontal axis is the detection time difference between STPL and the liquid scintillation detector. The time resolution of 2.7 ns (full width at half maximum) has enabled a good separation between neutron and γ-ray events.

D. Data acquisition

For each incoming fragment, the energy deposit in TRPL was monitored on-line. When the energy deposit was large enough to ensure $Z \geqslant 5$, the primary beam was turned off. Beta-decay events were then measured during the beam-off period, which lasted for 100 ms, a much longer period than the expected values of $t_{1/2}$. During this period, several β-ray

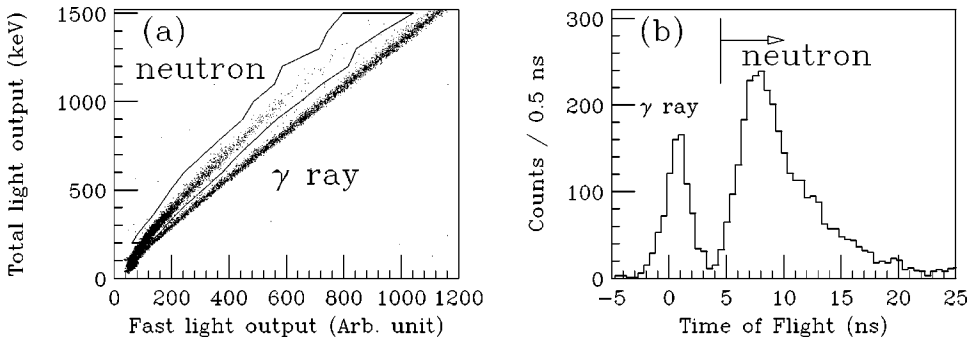

FIG. 3. Separation of neutrons and γ rays with the neutron detector array. (a) A two-dimensional plot of neutron-γ ray separation obtained for ^{15}B by pulse shape analysis. The vertical axis is the total light output in electron equivalent energy, and the horizontal axis is the amount of light output being integrated over the first 60 ns. The solid lines represent the neutron gate adopted for events with the electron equivalent energy $E_{eq}>200$ keV. (b) A spectrum of detection time differences between β rays and neutrons/γ rays for small light-output events of ^{15}B (50 keV$\leqslant E_{eq}\leqslant$200 keV). The arrow in the spectrum denotes the neutron gate adopted for the small light-output events.

events may occur in the sequence of chain decay and also accidentally. Supposing that only the first event would be accepted, the resultant decay curve would be distorted by the blocking effect on the succeeding events. To avoid such distortion, we performed a multiple recording of β-decay events during a single beam-off period using a nonstop TDC.

When a β ray was detected at STPL the time difference between the implantation and the β-ray detection was recorded to produce a decay curve spectrum. At the same time, the information from the neutron detectors on the detection time as well as their fast and total light outputs was recorded.

In an off-line analysis, the information on the β decay was associated with the specific implanted fragment which triggered the relevant beam-off period. In this way subsequent implantations of fragments were rejected during the β detection period, assuring a definite correlation between an implanted nucleus and the relevant β decay events.

III. DATA ANALYSIS

Decay curves were produced for β-ray events in singles and in coincidence with a single neutron. Decay curves were also obtained for two-neutron coincidence events when statics allowed. The values of $t_{1/2}$ and P_{in} were then determined by fitting the singles and coincidence decay curves simultaneously with a common set of parameters. In the analysis the effects of scattered neutrons were taken into account.

A. Decay curves

Figure 4 shows the decay curves obtained from singles and coincidence measurements for nuclei ^{19}B, ^{22}C, and ^{23}N. The singles spectrum can be decomposed into spectra for different coincidence conditions with neutrons. The spectra labeled by $A-in$ ($i=0$, 1, and 2) represent the spectra for parent nucleus A obtained by requiring coincidence with i neutron(s). To gain statistics all the events from the different RIPS settings were summed up.

In deducing $t_{1/2}$ and P_{in}, we only employed decay curves with sufficient statistics. Hence the decay curves of singles, β-1n, and β-2n coincidence were used for ^{19}B and ^{23}N, while only the first two were used for ^{22}C. Therefore, $t_{1/2}$, P_{1n}, and P_{2n} were deduced for ^{19}B and ^{23}N, while only $t_{1/2}$ and P_{1n} were obtained for ^{22}C.

B. Deduction of $t_{1/2}$ and P_{in}

In view of the relatively poor statistics, the method of maximum likelihood was applied for deducing the values of $t_{1/2}$ and P_{in}. Because of a large Q_β value, the initial β decay can be followed by a multiple emission of delayed neutrons, leading to different daughter isotopes. Furthermore, these daughter isotopes can also have a sufficiently large Q_β values so that they undergo successive β decays, occasionally even followed by delayed neutron emissions. Hence, the fitting function for the decay curve involved the $t_{1/2}$ and P_{in} values not only of the parent nucleus but also of its daughters. The $t_{1/2}$ values of the granddaughters are sufficiently long so that the corresponding contributions were treated as part of a constant background.

The fit was made to a set of the decay curves ($A-in$; $i=0$, 1, and 2) altogether. This method removed possible complication and inconsistency, which might occur if the different decay curves were fitted separately. In a separate analysis, a set of decay parameters was obtained from each of the decay curves. However, to achieve consistency among them would require a lengthy process of iteration, which may end up with an ambiguous conclusion. Thus we deduced the decay parameters by fitting all the decay curves simultaneously. In this method all the decay parameters were treated as the fitting parameters, and hence, the method enabled a direct deduction of the decay parameters with consistency among all the decay curves.

A search for the values of the parameters was made, using the fitting and uncertainty analysis code MINUIT [15]. To obtain a better convergence the number of free parameters was reduced as much as possible. Hence $t_{1/2}$ and P_{in} of the daughter nuclei were fixed at the central values taken from the literature [10]. The remaining free parameters then were $t_{1/2}$ and P_{in} of the parent nucleus and a constant background level for each of the decay curves. Moreover, the total registered number of the β disintegrations of the parent nucleus, N_0, was also taken as a free parameter.

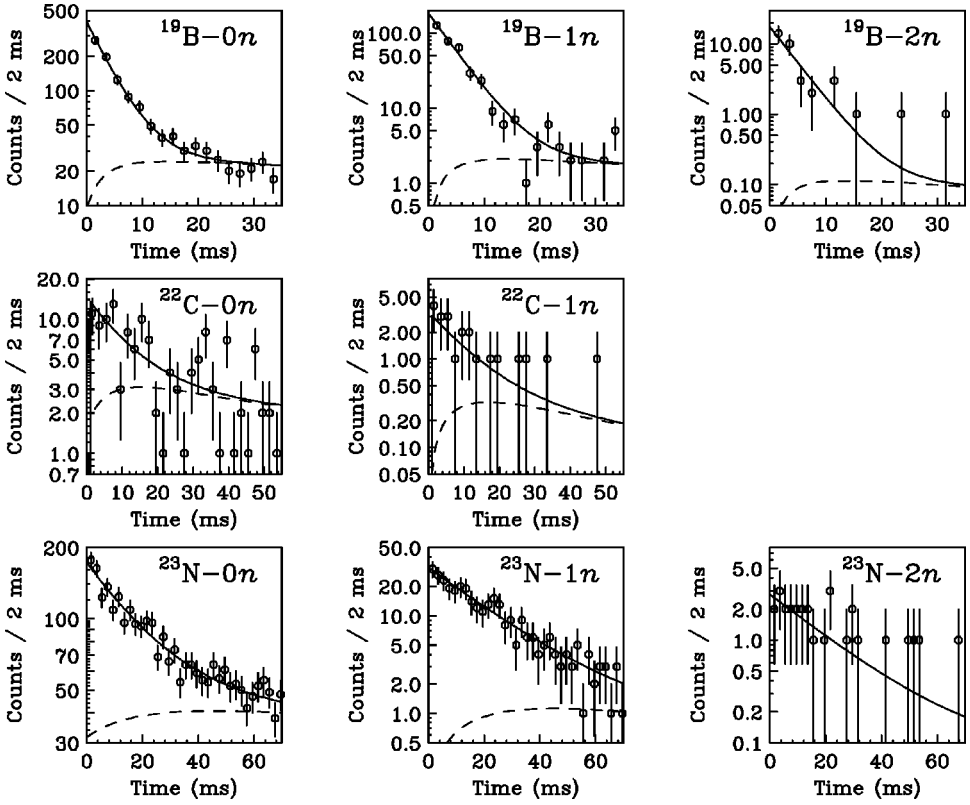

FIG. 4. The decay curves obtained for ^{19}B, ^{22}C, and ^{23}N. The decay curves for one neutron and two neutron coincidence events (1-n,2-n) are shown as well as for those events which were not in coincidence with any neutron (0-n). The solid lines represent the best-fit curves and the dashed lines the sum of the adopted backgrounds and daughter decay components.

The neutron detection efficiencies were treated carefully, since neutrons from the fragment arrived at the detectors after scattering as well as directly. The direct and scattered components have different detection efficiencies, ϵ and ϵ^*. Hence the probability of detecting p neutrons for an event with the neutron multiplicity M is expressed as [16]

$$\mathcal{E}_{Np}(M)=\binom{N}{p}\sum_{n=0}^{p}(-1)^{n+p}\binom{p}{n}[1-(N-n)\epsilon]^M \times[1-(N-n)\epsilon^*]^M, \quad (1)$$

where N represents the number of detectors used. Using the resulting $\mathcal{E}_{Np}(M)$ values, the total number of i-neutron coincidence events, N_i, was related to N_0 as follows:

$$N_i=N_0\times\sum_j \mathcal{E}_{Ni}(M=j)\times P_{jn}. \quad (2)$$

In order to determine the values of ϵ and ϵ^*, we performed a separate measurement using a beam of ^{15}B, which has the known values of $t_{1/2}=9.87\pm0.07$ ms [10], $P_{1n}=99.68^{+0.08}_{-1.58}$%, and $P_{2n}<1.5$% [11]. We fitted three decay curves of the singles, β-1n, β-2n coincidence events with parameters of $t_{1/2}$ of ^{15}B, ϵ, ϵ^*, and a constant background of each decay curve. The fitted value of $t_{1/2}$ is $9.86^{+0.15}_{-0.19}$ ms, which is in good agreement with the literature value, verifying the validity of the fitting procedure. The efficiencies ϵ and ϵ^* were deduced to be 2.423 ± 0.024% and $0.3644^{+0.012}_{-0.045}$%, respectively. They correspond to the total efficiencies of 31.5 ± 0.3% and $4.7^{+0.2}_{-0.6}$% when the direct and scattered neutrons were detected with the whole volume of the neutron detector array. It was assumed that this efficiency can be used for the decay of the nuclei presented in this paper as well.

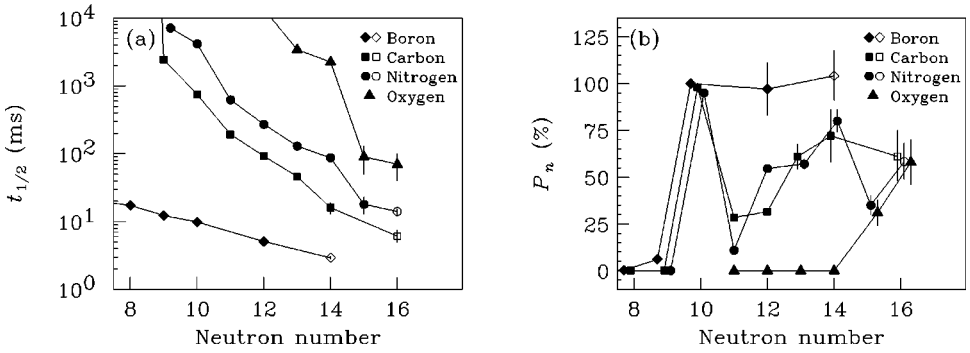

FIG. 5. The neutron-number dependence of $t_{1/2}$ (a) and P_n (b). The open symbols represent the results of the present work, and the filled ones the literature values [10]. A monotonic decrease of $t_{1/2}$ is seen in (a), while abrupt changes of P_n occur in (b), which may be due to the effect of the shell or subshell closure.

TABLE II. The experimental β-decay half-lives and β-delayed neutron multiplicities for the neutron-rich isotopes measured in this experiment. The upper limits correspond to the 90% confidence level. The results are compared with the available literature values.

Isotope	Half-life (ms)		β-delayed neutron multiplicities (%)	
	This work	Others	This work	Others
^{15}B	$9.86^{+0.15}_{-0.19}$	9.87 ± 0.07 [10]	($P_{1n}=99.68$)	$P_{1n}=99.68^{+0.08}_{-1.58}$ [11]
^{19}B	2.92 ± 0.13	4.5 ± 1.5 [4]	$P_{1n}=71.8^{+8.3}_{-9.1}$	-
			$P_{2n}=16.0^{+5.6}_{-4.8}$	-
			$P_{3n}<9.1$	-
^{20}C	$21.8^{+15.0}_{-7.4}$	16 ± 3 [5,6,10]	$P_{1n}=65^{+19}_{-18}$	$P_n=72\pm14$ [6,10]
			$P_{2n}<18.6$	-
^{22}C	$6.1^{+1.4}_{-1.2}$	-	$P_{1n}=61^{+14}_{-13}$	-
			$P_{2n}<37$	-
^{22}N	$16.5^{+8.5}_{-4.8}$	18 ± 5 [5,6,10]	$P_{1n}=41^{+12}_{-10}$	$P_n=35\pm5$ [6,10]
			$P_{2n}<13$	-
^{23}N	$14.1^{+1.2}_{-1.5}$	-	$P_{1n}=42.2^{+6.3}_{-6.5}$	-
			$P_{2n}=8.0^{+3.8}_{-3.4}$	-
			$P_{3n}<3.4$	-

IV. RESULTS AND DISCUSSIONS

The values of $t_{1/2}$ and P_{in} obtained from the present work are summarized in Table II together with the available literature values [4,6,10,11]. The quoted $t_{1/2}$ and P_{in} uncertainties are mainly due to the statistical ones, but also include systematic uncertainties due to the ambiguities in the fixed fitting parameters $t_{1/2}$ and P_{in} of the daughter nuclei and neutron detection efficiencies ϵ and ϵ^*. These systematic uncertainties were evaluated from separate fits in which these parameters were artificially shifted to their upper or lower bounds allowed by the literature values. The deviations between the central values and the original results were taken to be the systematic uncertainties. Because of the limited statistics, the P_{3n} values for ^{19}B and ^{23}N and the P_{2n} values for the rest of the isotopes were not determined. Instead, the upper limits with a 90% confidence level were obtained for these variables. It should be noted that the influence of the neutron energy cutoff on P_{in} values has been neglected.

The values of $t_{1/2}$ of ^{22}C and ^{23}N have been determined for the first time. A comparatively high precision of about 10% was achieved for these values. The $t_{1/2}$ value of ^{19}B has been determined with a much higher precision. The value indicates a shorter $t_{1/2}$ value than the previous result [4]. P_{in} values have been obtained for these three nuclei. In the present experiment the known decay properties of ^{20}C and ^{22}N have also been reexamined. For these isotopes, the experimental conditions were not optimized so that the accuracy of the results is relatively poor. The values obtained for $t_{1/2}$ and P_{in} are, however, in agreement with the literature values within the respective uncertainties. In Fig. 5 the present results of $t_{1/2}$ and P_{in} are compared with those of the neighboring nuclei. For all the isotopes plotted in Fig. 5(a), the value of $t_{1/2}$ decreases gradually as the neutron number increases.

Figure 5(b) shows plots of the neutron emission probability as a function of the neutron number. To allow for a comparison with the nearby nuclei, the total emission probability P_n, which is defined as the weighted sum of P_{in} ($P_n \equiv \Sigma_i i \times P_{in}$), is taken as the vertical coordinate. Abrupt changes of P_n are seen to occur at certain neutron numbers. It is likely that such changes are related to the shell (or subshell) closure, since P_n may be strongly influenced by the magnitude of the neutron separation energy (S_n) of the daughter nucleus. Indeed, a change occurs most strongly between the neutron number $N=9$ and 10 isotopes. For an $N=9$ parent nucleus, its daughter isotope has the magic number $N=8$, and hence a large S_n value. This leads to a wide opening to the energy window of the β-0n decay, thereby reducing the P_n value. For an $N=10$ isotope, the reduced S_n value of its

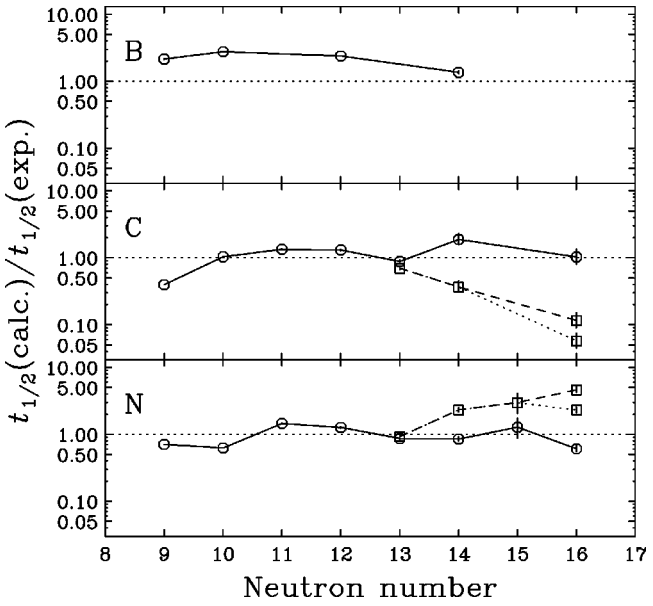

FIG. 6. A comparison of the theoretical and experimental β-decay half-lives of very neutron-rich boron, carbon, and nitrogen isotopes. The circles and solid lines refer to the semigross calculation [17,19], and the squares to the QRPA calculation [18] based on the mass formulas of Groote *et al.* (dashed lines) [20] and of Hilf *et al.* (dotted lines) [21].

daughter $N=9$ favors the delayed neutron emission. A similar behavior of P_n is observed to occur between the $N=15$ and 16 isotopes of nitrogen and oxygen. This may be related to the subshell closure at $N=14$ for the nitrogen and oxygen isotopes.

Finally, we compare the experimental values of $t_{1/2}$ with two sets of theoretical predictions so far available in the literature: the semi-gross theory (SGT) [17], and the proton-neutron quasiparticle random phase approximation (QRPA) [18]. The former employs the mass compilation in Ref. [19] based on experimental Q_β values, while it uses the theoretical mass prediction for the unknown Q_β values, i.e., for ^{19}B, ^{22}C, and ^{23}N. The latter uses the mass formula in Refs. [20,21] for all the mass values. In Fig. 6 the ratios of the theoretical values to the experimental values are plotted for boron, carbon, and nitrogen isotopes. The prediction of SGT reproduces the experimental data fairly well, while the QRPA prediction tends to deviate for larger neutron numbers. It is possible that the discrepancy between the two predictions may partly have arisen from the different sets of the mass values chosen.

V. SUMMARY

In summary, we have determined the half-lives and β-delayed neutron multiplicities of the neutron drip-line nuclei ^{19}B, ^{22}C, and ^{23}N, taking advantage of high efficient production of very neutron-rich nuclei at RIPS with a high-energy, high-intensity ^{40}Ar beam. The half-lives of ^{22}C and ^{23}N and the neutron multiplicities of ^{19}B, ^{22}C, and ^{23}N have been determined. The half-life of ^{19}B has been reexamined, yielding a value with a better precision.

ACKNOWLEDGMENTS

The authors would like to thank the staff of the RIKEN Ring Cyclotron for the stable operation of the accelerators during the experiment. We would also like to thank Dr. V. Kunze and his colleagues for their development of the neutron detector array. One of the authors (K.Y.) gratefully acknowledges the Japan Society for the Promotion of Science for a grant.

[1] H. Sakurai *et al.*, Phys. Lett. B **448**, 180 (1999).
[2] M. Notani *et al.*, Phys. Lett. B **542**, 49 (2002).
[3] H. Sakurai *et al.*, Nucl. Phys. **A616**, 311 (1997).
[4] A.T. Reed *et al.*, Phys. Rev. C **60**, 024311 (1999).
[5] M. Lewitowicz *et al.*, Nucl. Phys. **A496**, 477 (1989).
[6] A.C. Mueller *et al.*, Nucl. Phys. **A513**, 1 (1990).
[7] T. Kubo, M. Ishihara, N. Inabe, H. Kumagai, I. Tanihata, K. Yoshida, T. Nakamura, H. Okuno, S. Shimoura, and K. Asahi, Nucl. Instrum. Methods Phys. Res. B **70**, 309 (1992).
[8] H. Sakurai *et al.*, Phys. Rev. C **54**, R2802 (1996).
[9] K. Yoneda *et al.*, J. Phys. G **24**, 1395 (1998).
[10] G. Audi, O. Bersillon, J. Blachot, and A.H. Wapstra, Nucl. Phys. **A624**, 1 (1997).
[11] R. Harkewicz, D.J. Morrissey, B.A. Brown, J.A. Nolen, Jr., N.A. Orr, B.M. Sherrill, J.S. Winfield, and J.A. Winger, Phys. Rev. C **44**, 2365 (1991).
[12] J.A. Winger, B.M. Sherrill, and D.J. Morrissey, Nucl. Instrum. Methods Phys. Res. B **70**, 380 (1992).
[13] For example, A.C. Mueller *et al.*, Z. Phys. A **330**, 63 (1988).
[14] V. Kunze, W.-D. Schmidt-Ott, U. Bosch-Wicke, R. Bottger, and H. Klein, Nucl. Instrum. Methods Phys. Res. A **361**, 263 (1995).
[15] F. James and M. Roos, CERN library, D506, MINUIT.
[16] D. Alber, H. Grawe, H. Haas, and B. Spellmeyer, Nucl. Instrum. Methods Phys. Res. A **263**, 401 (1988).
[17] N. Nakata, T. Tachibana, and M. Yamada, Nucl. Phys. **A625**, 521 (1997).
[18] A. Staudt, E. Bender, K. Muto, and H.V. Klapdor-Kleingrothaus, At. Data Nucl. Data Tables **44**, 79 (1990).
[19] G. Audi and A.H. Wapstra, Nucl. Phys. **A595**, 409 (1995).
[20] H. von Groote, E.R. Hilf, and K. Takahashi, At. Data Nucl. Data Tables **17**, 418 (1976).
[21] E.R. Hilf, H. von Groote, and K. Takahashi, CERN-Report 76-13, 142 (1976).